

Completeness of Impact Monitoring

Alessio Del Vigna^{a,b}, Andrea Milani †, Federica Spoto^c, Andrea Chessa^b, Giovanni B. Valsecchi^{d,e}

^a*Dipartimento di Matematica, Università di Pisa, Largo Bruno Pontecorvo 5, Pisa, Italy*

^b*Space Dynamics Services s.r.l., via Mario Giuntini, Navacchio di Cascina, Pisa, Italy*

^c*IMCCE, Observatoire de Paris, PSL Research University, CNRS, Sorbonne Universités, UPMC Univ. Paris 06, Univ. Lille, 77 av. Denfert-Rochereau F-75014 Paris, France*

^d*IAPS-INAF, via Fosso del Cavaliere 100, 00133 Roma, Italy*

^e*IFAC-CNR, via Madonna del Piano 10, 50019 Sesto Fiorentino, Italy*

Abstract

The completeness limit is a key quantity to measure the reliability of an impact monitoring system. It provides the impact probability threshold for which every virtual impactor (VI) with impact probability above this value has to be detected. The completeness limit depends on the confidence region sampling: a goal of this paper is to increase the completeness without increasing the computational load, thus we propose a new method to sample the Line Of Variations (LOV) with respect to the previously one used in NEODYs. The step-size of the sampling is not uniform in the LOV parameter, since the probability of each LOV segment between consecutive points is kept constant. Moreover, the sampling interval has been extended to the larger interval $[-5, 5]$ in the LOV parameter and a new decomposition scheme in sub-showers and sub-returns is provided to deal with the problem of duplicated LOV points appearing in the same return.

The impact monitoring system CLOMON-2 has been upgraded with all these new features, resulting in a decrease of the impact probability IP^* corresponding to the generic completeness limit by a factor $\simeq 4$ and in an increase of the computational load by a factor $\simeq 2$. Moreover, since the generic completeness limit is an analytic approximation, we statistically investigate the completeness actually reached by the system. For this we used two different methods: a direct comparison with the results of the independent system Sentry at JPL and an empirical power-law to model the number of virtual impactors as a function of the impact probability. We found empirically that the number of detected virtual impactors with $IP > IP^*$ appears to grow according to a power-law, proportional to $IP^{-2/3}$. An analytical model explaining this power-law is currently an open problem, but we think it is related to the way the number of virtual impactors within a time t_{rel} from the first observed close approach accumulates. We give an analytical model and we prove that this cumulative number grows with a power-law proportional to t_{rel}^3 . The power-law allows us to detect a loss of efficiency in the virtual impactors search for impact probabilities near the generic completeness limit. The outcome of the comparison with Sentry shows that the two histograms of the number of VIs as a function of IP are very consistent for $IP > IP^*$, which supports the confidence in the reliability of both systems.

Keywords: Impact Monitoring, Generic completeness, Line Of Variations

1. Introduction

Some asteroids with an Earth-crossing orbit may impact our planet. A crucial issue is to be able to identify the cases that could have a threatening Earth close encounter within a century, as soon

Email address: delvigna@mail.dm.unipi.it (Alessio Del Vigna)

(†) During the final revision of this paper a tragedy occurred: Prof. Andrea Milani passed away on November 28, 2018. The present paper is dedicated to his memory.

as new asteroids are discovered or as new observations are added to prior discoveries. The main goal of impact monitoring is to solicit astrometric follow-up to either confirm or more likely dismiss the announced risk cases, *i.e.*, asteroids having some virtual impactors (Milani et al., 2000). This is achieved by communicating the impact date, the impact probability and the estimated impact energy.

This activity requires an automated system that continually monitors the Near-Earth Asteroids (NEAs) catalog. CLOMON-2² and Sentry³ are two independent impact monitoring systems that have been operational at the University of Pisa since 1999 and at JPL since 2002, providing the list of asteroids with a non-zero probability to impact the Earth within a century (Milani et al., 2005a). There is a constant comparison between the results of the two systems and, as required by the International Astronomical Union, the results are carefully cross-checked before any public announcement of an impact risk above an agreed level, as measured by the Palermo Scale (Chesley et al., 2002). There is a probability threshold called *generic completeness limit* that the two systems set as a goal. Above this threshold the search for impact possibility has to be complete, that is every virtual impactor (*i.e.*, each connected set of initial conditions leading to a collision with a planet) with an impact probability greater than the completeness limit has to be detected. Desirably, the generic completeness levels of the two concurrent impact monitoring systems need to be as close as possible, in order to have a common threshold down to which the two systems can be compared.

Since the generic completeness limit is a theoretical quantity, defined under some simplified assumptions, the level of completeness actually reached by the system has to be measured *a posteriori*. If the generic completeness limit in impact probability is somewhat lower than the actual level achieved, it means that there is a loss of efficiency in the VI search, that is some VI which could in theory be detected is missed in the scan. Finding possible causes and trying to decrease the number of missed VIs leads to an improvement of the whole system, filling as much as possible the gap between the two completeness limits. There are two methods to measure this quantity: the first is based on an empirical law to model the number of virtual impactors as a function of the impact probability; the second is a direct comparison with the results of an other independent system, namely Sentry, since we do not have a “ground truth”, that is a practical way to generate an absolutely complete list of all possible VIs above a given impact probability IP . We analyzed the results of the application of our new method by exploiting both the techniques.

2. The impact monitoring problem

The mathematical methods used in impact monitoring have been developed over the years, in a sequence of papers to which we refer the reader for a complete explanation: Milani et al. (1999), Milani et al. (2000), Chesley et al. (2002), Valsecchi et al. (2003), and Milani et al. (2005a).

The classical procedure to determine the orbit of an asteroid uses as initial condition at t_0 the solution $\mathbf{x}^* \in \mathbb{R}^N$ of a non-linear least squares fit, along with its covariance matrix $\Gamma := \Gamma(\mathbf{x}^*)$ (Milani and Gronchi, 2010, Chapter 5). We denote with N the dimension of the parameter space⁴.

²<http://newton.dm.unipi.it/neodys/index.php?pc=4.1>

³<http://cneos.jpl.nasa.gov/sentry/>

⁴The fit parameters space has dimension $N = 6$ when we solve for the six orbital elements, but it could have higher dimension if some other parameter is determined along with the orbital elements. A common situation is the determination of the Yarkovsky-related semimajor axis drift (Farnocchia et al., 2013; Chesley et al., 2016;

The nominal solution is surrounded by a set of orbits that are still compatible with the observational dataset, the so-called *confidence region*. It is the basic tool for the impact monitoring activity, since impact predictions have to take into account the nominal solution as well as its uncertainty, given by the matrix Γ . The confidence region can be approximated by the *confidence ellipsoid*

$$Z_{lin}(\sigma) := \{ \mathbf{x} \in \mathbb{R}^N : (\mathbf{x} - \mathbf{x}^*)^T C (\mathbf{x} - \mathbf{x}^*) \leq \sigma^2 \},$$

where $\sigma > 0$ is a confidence level and $C := \Gamma^{-1}$ is the normal matrix. Thus the confidence ellipsoid $Z_{lin}(\sigma)$ is the region delimited by the $(N - 1)$ -dimensional ellipsoid given by the positive definite quadratic form associated to the normal matrix C . As explained in what follows, the confidence ellipsoid is just used for local computations, since the assumptions to use this approximation are not applicable to impact monitoring in general.

2.1. Sampling of the confidence region

The main goal of impact monitoring is to establish whether the confidence region contains virtual impactors. Thus the confidence region is sampled by a finite set of *Virtual Asteroids* (VAs). Since the dynamical system describing the asteroid orbits is not integrable, only a finite number of VA initial conditions can be computed and propagated over the selected time interval. This sampling has to be done in an efficient way, that is with a few but selected orbits, in such a way that they are as much as possible representative of the infinite set of possible orbits. The geometric sampling methods are one possible way to select the ensemble of virtual asteroids: for this class of methods the sampling takes place on the intersection between the confidence region and a differentiable manifold. In particular, Milani (1999) and Milani et al. (2005b) introduced a 1-dimensional sampling method, in which the geometric object is a smooth line in the orbital elements space, the Line Of Variations. The main advantage of this approach is that the set of VAs has a geometric structure, that is they belong to a differentiable curve along which interpolation is possible.

Another sampling method, namely Monte Carlo, directly uses the probabilistic interpretation of the least squares principle, sampling the probability distribution in the orbital elements space to obtain a set of equally probable orbits (Chodas and Yeomans, 1996). More complex sampling methods, such as 2-dimensional ones, have been proposed in Tommei (2005) and have been recently used to deal with the problem of the imminent impactors (Farnocchia et al., 2015; Spoto et al., 2018).

2.2. LOV propagation

The LOV sampling computation provides a set of orbits $\{ \mathbf{x}(\sigma_i) \}_{i=-M, \dots, M}$, corresponding to values $\{ \sigma_i \}_{i=-M, \dots, M}$ of the LOV parameter. As introduced in Milani et al. (1999), the second step in impact monitoring consists in the propagation of each VA in the future. The close approaches of each VA with the Earth are recorded by means of sets of points on the Target Plane (TP), which is the plane passing through the Earth’s center and orthogonal to the unperturbed velocity of the asteroid⁵. To avoid geometric complications, we consider “close” only those approaches with

Del Vigna et al., 2018). This has consequences also for impact monitoring. Indeed, a dynamical model including non-gravitational forces is sometimes needed to make reliable impact predictions, especially if the hazard analysis time span is extended to time intervals longer than one century.

⁵That is, orthogonal to the incoming asymptote of the hyperbola defining the two-body approximation of the trajectory at the time of closest approach (Valsecchi et al., 2003).

a distance from the Earth center of mass not exceeding some value R_{TP} . Possible values for R_{TP} range between 0.05 au and 0.2 au, thus the target planes are in fact disks with a finite radius.

The first output of the LOV propagation is a collection of Earth encounters that have been detected for each VA during the time span of interest. Each close approach with initial condition \mathbf{x}_i is represented by at least one trace $\mathbf{y}_i = (\xi_i, \zeta_i)$ on the corresponding target plane⁶.

2.3. Stretching and width

Let us denote with $\mathbf{g} : \mathbb{R}^N \rightarrow \mathbb{R}^2$ the function mapping an orbit \mathbf{x} at epoch t_0 to the point \mathbf{y} on the TP of an encounter occurring at an epoch t_1 . This map is the composition of the propagation from t_0 to t_1 and of the projection on the target plane. In the linear approximation, which is justified since the return analysis is performed locally, the confidence ellipsoid $Z_{lin}^X(\sigma)$ around \mathbf{x}^* is mapped onto a confidence ellipse $Z_{lin}^Y(\sigma)$ around $\mathbf{y}^* = \mathbf{g}(\mathbf{x}^*)$. By applying the covariance propagation law, the target plane ellipse is defined by

$$(\mathbf{y} - \mathbf{y}^*)^T C_{\mathbf{y}} (\mathbf{y} - \mathbf{y}^*) \leq \sigma^2,$$

where $C_{\mathbf{y}} = \Gamma_{\mathbf{y}}^{-1}$ and $\Gamma_{\mathbf{y}} = D_{\mathbf{x}^*} \mathbf{g} \Gamma_{\mathbf{x}} (D_{\mathbf{x}^*} \mathbf{g})^T$. The square roots of the eigenvalues of $\Gamma_{\mathbf{y}}$ are the semimajor and semiminor axis of $Z_{lin}^Y(1)$, respectively called *stretching* and *width*.

If we have a LOV sampling, as in the case of impact monitoring, we have a further map $\mathbf{s} : \mathbb{R} \rightarrow \mathbb{R}^N$, which is the parameterization of the LOV as a differentiable curve, that is $\mathbf{s}(\sigma_i) = \mathbf{x}_i$. In this way we can consider the composite map $\mathbf{f} := \mathbf{g} \circ \mathbf{s}$ from the sampling space to the target plane and define the *stretching along the LOV* in σ as

$$S(\sigma) := \left| \frac{d\mathbf{f}}{d\sigma}(\sigma) \right|. \quad (1)$$

The stretching along the LOV measures the displacement of two points on the target plane as a function of the separation between the corresponding points in the sampling space.

2.4. Return analysis

If the close encounter collection is not empty, the first step in the decomposition is to sort the encounters by date, followed by a splitting into *showers* that are clustered in time. The showers are then divided into contiguous LOV segments: the shower encounters are re-sorted according to their LOV index, and then, advancing through the sorted list, we “cut” the shower wherever a gap in the LOV index is encountered. We call *returns* these sets of dynamically related encounters. After the entire propagation, each close approach is carefully analyzed to search for virtual impactors.

When there are many points on the TP in a given return it is easy to understand the LOV behavior: the stretching is small and the linear theory is locally applicable. On the contrary, in strong non-linear cases the stretching is large and changes rapidly from point to point: in this case a local analysis is necessary in the neighborhood of each VA. We refer to Milani et al. (2005a); Tommei (2006) for a discussion on the possible geometries of the LOV trace on a target plane and for a proper solution for each case. Here we only want to outline the basic idea of the return analysis with a simple example. The key point is that the virtual asteroids are not just a set of points but they sample a smooth curve, allowing us to interpolate between consecutive sample

⁶For a discussion on the choice of the coordinates (ξ, ζ) on the TP, see Valsecchi et al. (2003); Milani et al. (2005a).

points. For instance, let us suppose two consecutive VAs \mathbf{x}_i and \mathbf{x}_{i+1} have TP trace points \mathbf{y}_i and \mathbf{y}_{i+1} straddling the Earth impact cross section. If the geometry of the TP trace is simple enough (principle of simplest geometry), an interpolation method provides a point on the LOV $\mathbf{x}_{i+\delta}$ with $0 < \delta < 1$ and such that $\mathbf{y}_{i+\delta}$ is inside the Earth impact cross section: then, around $\mathbf{x}_{i+\delta}$ there is a virtual impactor. If a virtual impactor has been found, by computing the probability density function with a suitable Gaussian approximation centered at $\mathbf{x}_{i+\delta}$ it is possible to estimate the probability integral on the impact cross section, that is the impact probability associated with the given VI.

2.5. Generic completeness definition

This paper is focused on the completeness of impact monitoring, that is on the completeness of the VI search. The *completeness limit* can be formally defined as the highest impact probability VI that can escape the detection. Given the complexity of the problem of impact monitoring, this completeness cannot be computed and thus we use an approximate definition, which assumes idealized circumstances. The *generic completeness limit* is the highest impact probability VI that could possibly escape detection, if the associated return on the target plane is fully linear (Milani et al., 2005a), that is under the hypothesis of full linearity of the map \mathbf{f} . Under this generic assumption the trace of the VAs on the target plane is simply a straight line on the TP: if there is a VI, this line intersects the impact cross section D on the TP in a chord of the circle bounding D .

For a VI to be detectable by the system, at least one LOV orbit has to cross the target plane. For now, we make the assumption that one point on the TP is sufficient for the VI detection (see Section 4 for a discussion on this choice). The stretching is a key quantity to estimate the number of LOV orbits that intersects the target plane of a given encounter: the higher is the stretching, the greater is the separation between two consecutive points on the TP. In particular, if the stretching becomes too high, the separation on the TP could exceed the diameter $2R_{TP}$ of the TP itself, thus no point crosses the TP and the virtual impactor is not detected with certainty. As a consequence, to have at least one point on the TP, the stretching cannot exceed a maximum value S_{max} . Assuming a uniform step-size $\Delta\sigma$ for the LOV sampling, the condition $S \cdot \Delta\sigma \leq 2R_{TP}$ must hold, which implies

$$S \leq \frac{2R_{TP}}{\Delta\sigma} =: S_{max}. \quad (2)$$

We now convert the previous inequality into a condition concerning the impact probability. The probability density function induced on the LOV by the probability density function on the orbital elements space⁷ is

$$p(\sigma) := \frac{1}{\sqrt{2\pi}} e^{-\frac{\sigma^2}{2}}, \quad (3)$$

where σ is the LOV parameter. Under our assumptions, the impact probability of the VI is given by integrating $p(\sigma)$ over the inverse image of the diametrical chord contained in the LOV projection on the TP. Assuming that the stretching is S , the integration domain is an interval with length $2b_{\oplus}/S$ in the σ -space. As a consequence, the following estimation holds:

$$IP \simeq \frac{2b_{\oplus}}{S} \cdot p(0) \geq \frac{1}{\sqrt{2\pi}} \frac{2b_{\oplus}}{S_{max}} = \frac{\Delta\sigma}{\sqrt{2\pi}} \cdot \frac{b_{\oplus}}{R_{TP}}.$$

⁷The probability density defined on the orbital elements space is the propagation of the Gaussian density assumed for the residuals, and it is Gaussian with mean \mathbf{x}^* (the nominal solution) and covariance matrix $\Gamma = \Gamma(\mathbf{x}^*)$, the covariance matrix of the orbit determination least squares fit (Milani and Gronchi, 2010).

where b_{\oplus} is the radius of the Earth impact cross section on the TP, which takes into account the gravitational focusing (Valsecchi et al., 2003). Since the generic completeness limit IP^* is the minimum impact probability of a VI for which condition (2) is satisfied, we have

$$IP^* := \frac{\Delta\sigma}{\sqrt{2\pi}} \cdot \frac{b_{\oplus}}{R_{TP}}.$$

This quantity depends on the amount of gravitational focusing, and can be higher for asteroids with a low velocity at infinity. To obtain a uniform threshold, we can use a typical value for b_{\oplus} , *e.g.*, $b_{\oplus} = 2R_{\oplus}$. This is an approximation, but we need to chose a fixed value applicable to all asteroids with VIs, thus we are using a value appropriate for low relative velocity NEA, taking into account that these have larger probability of having VIs. In this way we have an approximated value for the generic completeness limit:

$$IP^* = \frac{\Delta\sigma}{\sqrt{2\pi}} \cdot \frac{2R_{\oplus}}{R_{TP}}. \quad (4)$$

With the previous simple equation we can provide an estimate of the completeness reached by CLOMON-2 while it was operating with a uniform LOV sampling. As shown in Milani et al. (2005a), we obtain⁸

$$IP^* \simeq 4.24 \cdot 10^{-7},$$

corresponding to a maximum stretching value of $S_{max} = 3.8 \cdot 10^6 R_{\oplus}$. In the case at least two points on the TP are required for the detection of a VI, the generic completeness limit IP^* would be simply twice as much.

3. An optimal method for LOV sampling

Before the switch to the new method presented in this paper, CLOMON-2 performed the LOV sampling by means of uniformly spaced points in the parameter σ , and over the interval $|\sigma| \leq 3$. Since the probability density on the LOV is the Gaussian defined by (3), a uniform step in σ is not optimal because the probability of each sampling interval is high around $\sigma = 0$, whereas it becomes too low near the LOV endpoints. This is the reason to use a step-size that is inversely proportional to the probability density. The new sampling is such that the probability of the interval among two consecutive points of the sampling is constant. It means that if $\{\sigma_i\}_{i=1, \dots, M}$ are the sampling nodes, then

$$\mathbb{P}([\sigma_i, \sigma_{i+1}]) := \int_{\sigma_i}^{\sigma_{i+1}} p(\sigma) d\sigma$$

is constant, *i.e.*, it does not depend on i . As a consequence, the sample points will be more dense around the value $\sigma = 0$ (nominal solution) whereas they become more sparse moving towards the tips. Furthermore, to avoid too long intervals at LOV tails, when the interval length exceeds a certain threshold $\Delta\sigma_{max}$ the sampling becomes uniform to the threshold value. This technical detail is needed to bound the step-size, since too large values of $\Delta\sigma$ could result in divergence of the algorithms to find VIs, effectively cutting the LOV tails out from the analysis. To avoid this

⁸The TP radius adopted for the close approaches detection was $R_{TP} = 0.2 \text{ au} \simeq 4700 R_{\oplus}$, the LOV sampling was performed with 2401 virtual asteroids over the interval $|\sigma| \leq 3$, thus $\Delta\sigma = 0.0025$.

loss and also to keep a better control of the cases in which a geometrically large VI occurs for large values of σ , the sampling interval has been extended to $|\sigma| \leq \sigma_{max} = 5$ (and also to cover the same interval as JPL's Sentry system).

We now derive a condition for the step-size to guarantee a constant probability to each sampling interval. This is achieved by repeating the same argument of Section 2.5, not around the nominal solution, but around the VA corresponding to a generic σ value. In particular, to have at least one point on the TP corresponding to the LOV parameter σ , the stretching must satisfy the condition

$$S(\sigma) \leq \frac{2R_{TP}}{\Delta\sigma(\sigma)} =: S_{max}(\sigma).$$

Under linearity assumptions, the impact probability of the VI around the value σ of the LOV parameter is given by

$$IP(\sigma) \simeq \frac{2b_{\oplus}}{S(\sigma)} \cdot p(\sigma) \geq \frac{2b_{\oplus}}{S_{max}(\sigma)} \cdot p(\sigma).$$

By assuming $b_{\oplus} = 2R_{\oplus}$ as above, we can define

$$IP^*(\sigma) := \frac{2R_{\oplus}}{R_{TP}} \Delta\sigma(\sigma) p(\sigma), \quad (5)$$

which is the minimum probability of a detectable VI around the value σ of the LOV parameter. To ensure the detection of a VI with probability $IP^*(\sigma)$ for all $|\sigma| \leq \sigma_{max}$, we have to define the generic completeness as

$$IP^* := \sup_{|\sigma| \leq \sigma_{max}} IP^*(\sigma).$$

Notice that we can take the supremum since $IP^*(\sigma)$ are bounded from above. Using (5), this implies the following condition on the step-size:

$$\Delta\sigma(\sigma) \leq \frac{R_{TP}}{2R_{\oplus}} IP^* \frac{1}{p(\sigma)}.$$

The computation of $\Delta\sigma_i := \Delta\sigma(\sigma_i)$ starts from the value $\sigma_0 = 0$ (corresponding to the nominal solution), and by recursion we compute

$$\begin{cases} \Delta\sigma_i = \min \left(\frac{R_{TP}}{2R_{\oplus}} IP^* \frac{1}{p(\sigma_i)}, \Delta\sigma_{max} \right), & i \geq 0 \\ \sigma_{i+1} = \sigma_i + \Delta\sigma_i, & i \geq 1 \end{cases} \quad (6)$$

for the sampling of the interval $0 \leq \sigma \leq \sigma_{max}$. For the negative side, that is the interval $-\sigma_{max} \leq \sigma \leq 0$, the nodes are $\{-\sigma_i\}_{i \geq 0}$. By definition of IP^* , the step-size is such that the inverse image of the diametrical chord has the same probability for all σ . And this in turn implies that each sampling interval has the same probability. Of course this holds only for the intervals with length not exceeding $\Delta\sigma_{max}$.

The new method allows one to choose the completeness limit before the sampling procedure starts. Thus the number of VAs per LOV side is known only at the end of the procedure (6), since it stops when σ_{max} is exceeded. This is somewhat different with respect to the previous method, for which we first established the number of VAs per LOV side and as a consequence the completeness level was determined, as in equation (4). Figure 1 shows the behavior of the step-size as a function

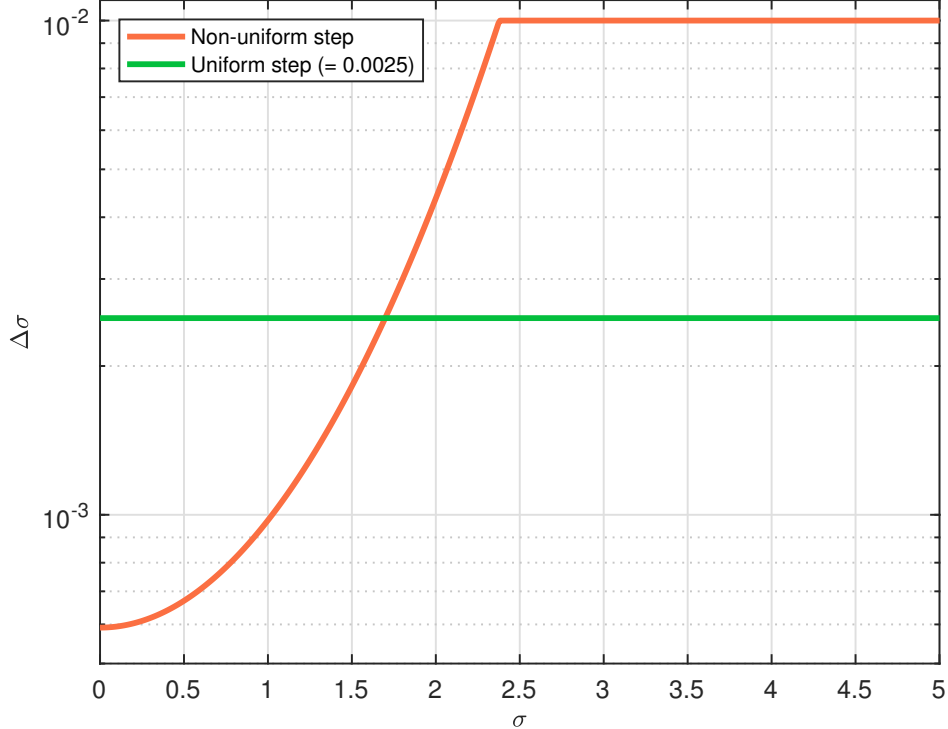


Figure 1: Graph of the step-size as a function of the LOV parameter σ , with the parameter choice as in (7). *Orange line*: step-size for the uniform-in-probability sampling. *Green line*: uniform step-size, as previously used by CLOMON-2.

of the LOV parameter σ . It was generated using the following values, which are the same used for the current impact monitoring computations:

$$IP^* = 1 \cdot 10^{-7}, \quad \sigma_{max} = 5, \quad \Delta\sigma_{max} = 0.01. \quad (7)$$

This choice of parameters leads to the computation of at most 4719 multiple solutions⁹, whereas at most 2401 VAs were computed with the previous sampling method (Milani et al., 2005b). This gives about twice the computational load than before, that however permits a decrease by a factor $\simeq 4$ in the generic completeness limit, since the value corresponding to the previous uniform sampling was $IP^* \simeq 4.24 \cdot 10^{-7}$, as computed in Section 2.5.

4. Missing VI detection: possible causes

Once a generic completeness level IP^* has been established, the goal is to find all the virtual impactors with probability $IP > IP^*$. This might not be achieved in actual computations in case some VI is not detected by the scan. In general, the identification of the causes and the development of possible solutions are important issues. We were aware of two possible sources of VI loss: in what follows we discuss both of them.

⁹The number of VAs may actually be lower, because we terminate the sampling when the residuals become too large, currently when $\chi > 5$.

4.1. Duplicated points in the same return

In Section 2.4 we have defined showers and returns as particular dynamically related subsets of the set of close encounters of all the virtual asteroids. The associated iterative procedure properly works as long as the showers are well-defined. Indeed, there are cases in which there is not a clear clustering in time among the encounters, causing the presence of very long showers (also called extended showers) in the decomposition. As a consequence, some virtual asteroids appear multiple times in the same return, and this must be avoided for the subsequent TP analysis to be successful. In general, several phenomena may cause this problem, for instance temporary capture of the asteroid by the Earth, Earth-like orbit (as for 2000 SG₃₄₄) and encounters with low relative velocity. There are also cases in which a close approach, defined in time as the interval in which the distance from the encountered body is less than some D_{min} (for the Earth $D_{min} = 0.2$ au), contains multiple occurrences of a local minimum distance, and this also generates returns with duplicated points. Such bad cases are not so rare as one may think, especially if we use a denser LOV sampling. The problem affects $\simeq 25\%$ of the asteroids in the NEODyS risk list (as of April 2018).

An example of such situation is given by asteroid 2000 SG₃₄₄, already used to present the problem of duplicated virtual asteroids in Milani et al. (2005a), Figure 6. We show a figure which cannot be identical to the one in Milani et al. (2005a) since, even if the observational data set is exactly the same, it is currently treated with a different astrometric error model. Figure 2 shows a single extended shower for 2000 SG₃₄₄ lasting for about one year. In this situation the previous algorithm identifies a single shower around the year 2069. Figure 2 shows the closest encounter date of the points belonging to the extended shower, against the LOV index. The clustering into returns is clear from the picture, but there are returns with multiple occurrence of the same virtual asteroid, as highlighted in orange.

To handle such cases, we decided to introduce a further splitting procedure every time a return contains duplicated virtual asteroids. This leads to the definition of sub-showers and sub-returns. First, we sort the return by ascending closest approach time, then we scan and divide it as follows: we cut the return every time a virtual asteroid is already present among the previous ones, starting from the previous cut. Each subset obtained in this way is called a *sub-shower*. Second, each sub-shower is divided into contiguous LOV segments, called *sub-returns*, in the same way we obtain the returns from the showers. Appendix A contains a mathematical description of the procedure just described, with a formal proof of completion. Thus the decomposition algorithm ensures that each sub-return is free from duplicated virtual asteroids. Then we use, as returns of the original shower, all the sub-returns of all the sub-showers. Figure 3 shows the outcome of the application of the splitting procedure to the return going from LOV index 1414 to 2779. As a graphical representation of the algorithm, we pass a horizontal line from the bottom to the top of the plot to scan the return by ascending closest approach time and we make a cut when we encounter a duplication. The return is decomposed into three sub-showers (represented with different marks and colors), each of which is further decomposed in contiguous LOV segments.

It is apparent from Figure 3 that our algorithm splits more than the minimum possible, *e.g.*, in this figure it can be seen that there are two cuts splitting dynamically related encounters (the second and third horizontal lines starting from the bottom). However, this has no negative consequences on the performance of the VI detection, because even the LOV interval between the last index of a sub-return and the first of the next is actually scanned, by using the algorithms for the tail and head of the return (Milani et al., 2005a). The split is different from the one performed by Sentry,

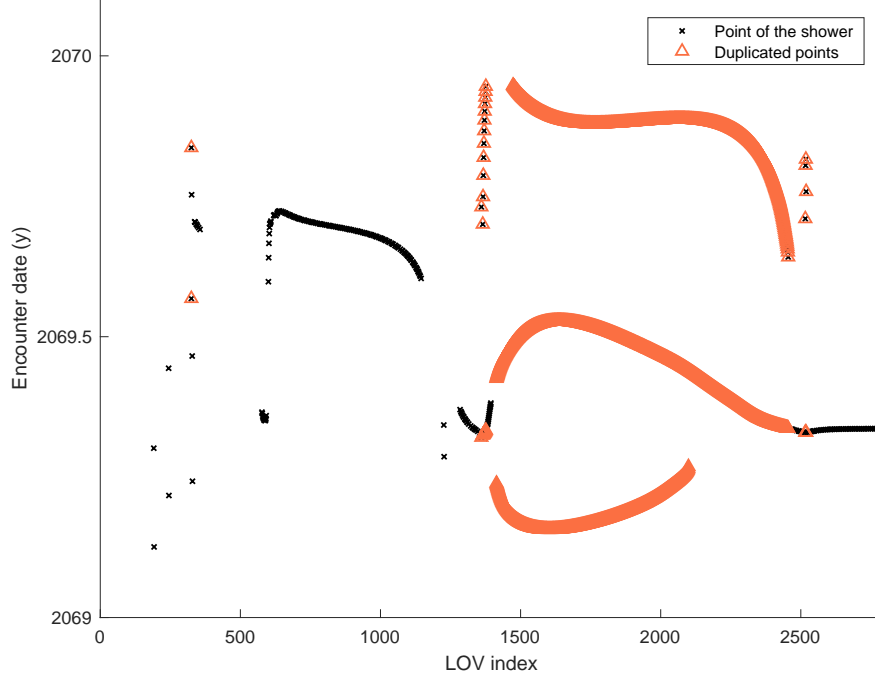


Figure 2: Extended shower around the year 2069 for asteroid 2000 SG₃₄₄. For each virtual asteroid belonging to the shower, we plot the closest encounter date against the LOV index (black crosses). The virtual asteroids that appear more than one times in the same return are highlighted (orange triangles).

but the result in terms of impact monitoring is the same.

In the work carried out for the switch to the new sampling of the Line Of Variations, we implemented the splitting procedure into sub-showers and sub-returns, thus the results presented in Section 5 take already into account also this improvement.

4.2. Extreme non-linear cases

When there is a strong non-linearity due to previous close approaches, the stretching is large and rapidly varying, causing the LOV behavior to be complex. Thus strong non-linearity of the map \mathbf{g} introduced in Section 2.3 can lead to unsuccessful detections of virtual impactors.

Inside a return, only some intervals between consecutive VAs can contain a minimum of the closest approach distance and they are identified by a geometric classification (Milani et al., 2005a). The analysis continues by checking if the minimum distance could be small and, if so, by applying iterative schemes and interpolation along the LOV to determine the minimum distance and the corresponding LOV orbit, respectively. In most cases, both CLOMON-2 and Sentry use the *modified regula falsi* applied to the continuous function

$$f(\sigma) := \frac{dr^2}{d\sigma}(\sigma)$$

over the interval $[\sigma_1, \sigma_2]$ under consideration, where $r^2(\sigma) := \xi^2(\sigma) + \zeta^2(\sigma)$ is the square of the distance from the Earth center. This algorithm is convergent, but failures may occur if for some value of σ in the interval the function is undefined. It happens when the TP of the encounter

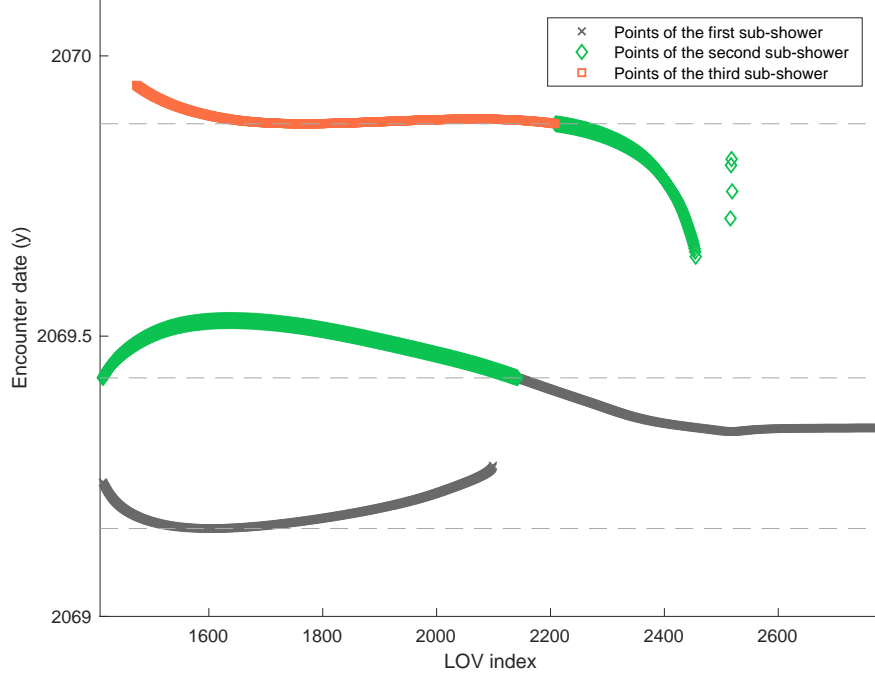


Figure 3: Application of the decomposition procedure to a return of the extended shower of 2000 SG₃₄₄. The return is decomposed into three sub-showers, represented with different marks and colors (orange, green, and gray, respectively). We mark with a black circle the first point (in terms of time) of each sub-shower: in particular, the first LOV indices of the three sub-showers are 1604, 1414 and 1766, respectively.

around that date is missed, which generally indicates that the two TP points under consideration do not actually belong to the same return (Milani et al., 2005a).

Another typical situation that may determine an unsuccessful detection is caused by singletons. They are returns consisting of one single point on the target plane, due to a very high value of the stretching at the corresponding LOV point and indicating an extremely non-linear situation. By definition the modified *regula falsi* cannot be applied in this case. The solution adopted by CLOMON-2 is the Newton method with bounded steps (Milani et al., 2005a): this method cannot diverge, but can fail to converge either by finding a value of σ for which the TP is missed, as in the previous case, or by exceeding a preset maximum number of iterations without achieving convergence with the required accuracy. In both cases there is the possibility that a VI actually exists in the analyzed LOV segment, but the method fails in detecting it. A possible solution to deal with this problem is to resort to a densification technique. If we suitably densify the LOV sampling around the orbit corresponding to the singleton and obtain a return with 4-5 points on the target plane instead of a lone point, this makes the TP analysis easier and more effective. Indeed, Figure 5 shows that the power-law fits well only for values of IP corresponding to at least 4 points on the TP: this is a further motivation for the use of a densification technique also for returns with very few points, although singletons remain the primary motivation for densification. We did not implement the densification of the sampling, though we intend to include it in our future work as discussed in Section 8.

5. Results

After the switch to the new sampling method, the actual level of completeness reached by the system has to be measured and compared with the one corresponding to the previous method. To perform this analysis we make use of the histograms of the number of virtual impactors \mathcal{N} as a function of the inverse of the impact probability IP (for the sake of clarity we used $\log_{10}(1/IP)$ on the horizontal axis). We made a histogram for the ensemble of VIs obtained using a uniform step-size in σ (previous sampling method employed by CLOMON-2) and a second one for the results of the new sampling method, uniform in probability, on the same set of asteroids, with the observations available at the same date. We used the data contained in the NEODyS database¹⁰ immediately before and after CLOMON-2 switched to the new method, namely on 29 October 2016. As a sample, we used the 571 asteroids in the NEODyS Risk List at that time, thus computed with the uniform sampling in the LOV parameter σ . As a result of the application of the new method we obtain a set of 558 asteroids with virtual impactors out of 571. The two histograms are shown in Figure 4 and 5 (left panel). The first thing that stands out is the very different total number of virtual impactors: the application of the new method almost doubled this number, causing an increase from 13604 to 25942 virtual impactors.

In both the histograms there are two vertical lines corresponding to two different values of impact probability:

- the orange line (the one on the right) represents the impact probability corresponding to the assumption that a VI is detectable with at least one target plane point (which is the minimum requirement), in full linear conditions;
- the red line (the one on the left) represents the impact probability corresponding to the assumption that at least two target plane points are needed for the detection of a virtual impactor.

The part of the histogram on the left of the orange line corresponds to $IP > IP^*$, namely to the impact probabilities of the virtual impactors that the system should detect with certainty. The number of virtual impactors \mathcal{N} is expected to grow as the impact probability goes down to IP^* . Even looking just to the histogram bars we notice that the growth of \mathcal{N} seems to slightly slow down close to the vertical lines with respect to what one would expect. To highlight this behavior we fitted the histogram contour for $IP > IP^*$ with a suitable law: the best-fit line is represented in light blue in both plots of Figure 4 and 5 (left panel) and it was obtained with a linear correlation coefficient > 0.99 in both cases. In particular, we performed a linear fit of the histogram contour in a log-log scale: Figure 4 and 5 (right panel) show the points corresponding to the histogram bar tips, those selected for the fit, and the best-fit line. A linear fit in the log-log plot corresponds to a power-law for the number of virtual impactors, that is

$$\mathcal{N} = n(IP) = c_1 \cdot \left(\frac{IP^*}{IP}\right)^\alpha \quad \text{if } IP \geq IP^*. \quad (8)$$

As a result we obtained the estimation $\alpha \simeq 0.678$ for the histogram related to the uniform sampling, and $\alpha \simeq 0.664$ for the histogram related to the uniform-in-probability sampling. These results are

¹⁰<http://newton.dm.unipi.it/neodys/>

remarkably close, even if obtained with different sampling of the LOV. Furthermore, other results of this paper (see Section 6 and Section 7) seem to confirm this numerical evidence. At this point we are still not able to provide a full interpretation of the value of $\alpha \simeq 2/3$ as a mathematical property of the ensemble of all the VIs. Nevertheless, as a first step in this direction, in Section 6 we outline a possible model to explain the growth of the number of virtual impactors \mathcal{N} as a function of the time.

For $IP < IP^*$, the probability to find a virtual impactor with impact probability IP is roughly the ratio IP/IP^* . Thus the number of virtual impactor is

$$\mathcal{N} = n(IP) \frac{IP}{IP^*} = c_1 \cdot \left(\frac{IP^*}{IP} \right)^{\alpha-1} \quad \text{if } IP < IP^*.$$

This equation corresponds to the descending green line in both plots. We notice that this line does not fit the right side histogram contour: there are more virtual impactors than expected from this law. For the results obtained with the new sampling, this can be explained by considering that the LOV sampling returns to be uniform in σ close to the LOV tails, and thus in that region the LOV is over-sampled with respect to what would be needed to reach the completeness level IP^* . With the old sampling, the production of VIs with low impact probability is still larger, because the sampling was not optimized specifically for $IP > IP^*$.

The differences between the fitted ascending curve corresponding to equation (8) and the histogram clearly show that there is a loss of efficiency in finding virtual impactors with impact probability slightly above the completeness level. Indeed, for these impact probability values the expected number of VIs based on the empirically fitted power-law is larger than the number of actually detected ones. To define the generic completeness limit we make the assumption that even a single point on the target plane allows the system to detect the virtual impactor, but from a practical point of view this completeness level cannot be reached due to non-convergence of the iterative schemes in some difficult cases, as explained in Section 4. Actually, this does not happen only with a single point on the target plane (singleton), but even with very few points. As discussed in Section 8, a densification of the LOV sampling is the way to fill the gap between the actual completeness level and the theoretical generic completeness. A possible densification technique could convert returns with very few points into return with 4-5 points. As a result, the iterative methods used (such as *regula falsi* and Newton's method with bounded steps) should converge in a larger number of cases and the VI search could be more efficient and complete.

6. Analytical formulation for the time evolution

We analyze the behavior of the cumulative number of virtual impactors \mathcal{N} as a function of the time elapsed from the initial conditions. As starting sample we used all the asteroids in the NEODyS Risk List (as of April 2018), which contained 734 objects and 32906 virtual impactors, without considering the special cases¹¹. The histograms of Figure 6 show the distribution of the inclination i and of the absolute magnitude H among the considered objects. As clear from simple arguments, the majority of the sample contains small low-inclination asteroids: for instance, 95.5% of the sample has absolute magnitude $H > 22$ and 71% has inclination $i < 5$ deg.

¹¹The four special cases are (101955) Bennu, (99942) Apophis, (29075) 1950 DA, and (410777) 2009 FD. These are currently the only asteroids that required the inclusion of the Yarkovsky effect for the impact monitoring.

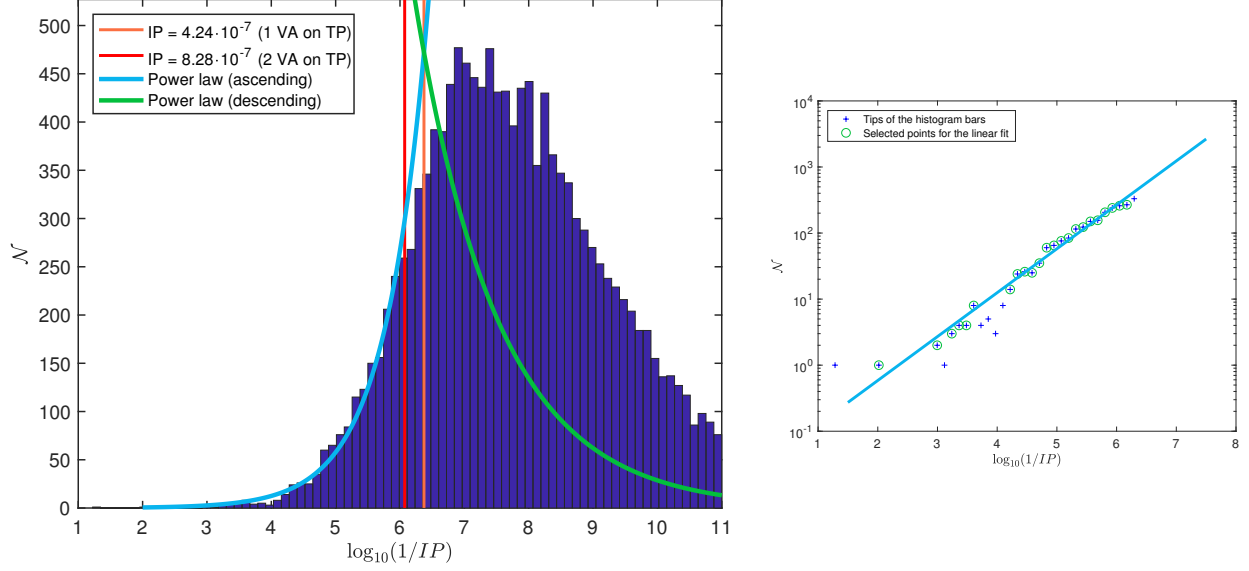


Figure 4: *Left panel.* Histogram of the number of virtual impactors (as of October 2016) as a function of the inverse of the impact probability, in the case of uniform sampling in σ . *Right panel.* Log-log plot of the histogram bar tips and corresponding regression line, providing $\alpha \simeq 0.678$.

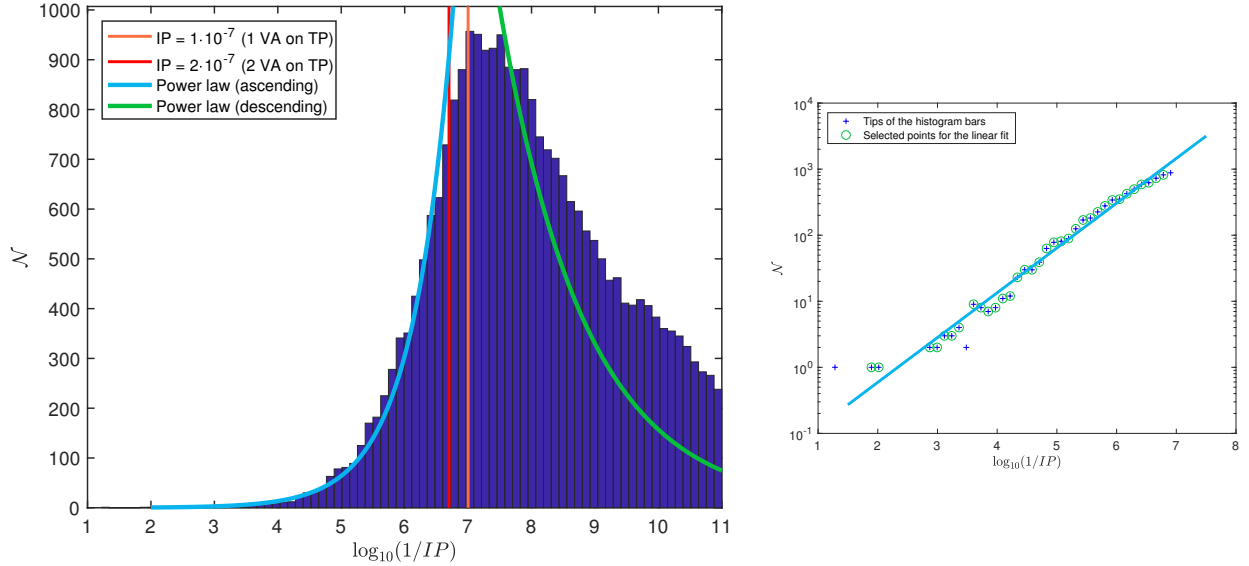


Figure 5: *Left panel.* Histogram of the number of virtual impactors (as of October 2016) as a function of the inverse of the impact probability, in the case of uniform-in-probability sampling. *Right panel.* Log-log plot of the histogram bar tips and corresponding regression line, providing $\alpha \simeq 0.664$.

The sample of virtual impactors for the time evolution has to be complete, that is it has to contain all the possible virtual impactors with IP down to a certain threshold. Thus the results of the new sampling of the LOV are a good starting point, since the new method ensures a complete virtual impactors search down to $IP^* = 1 \cdot 10^{-7}$. To take into account the loss of completeness due to singletons, as discussed in Section 4 and 5, we selected the virtual impactors with $IP > 2 \cdot 10^{-7}$:

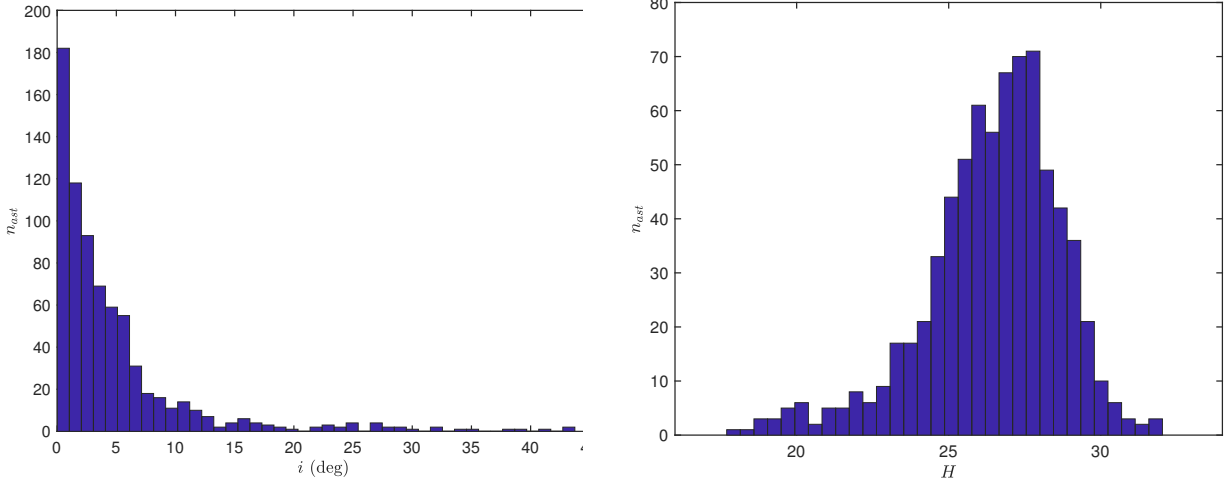


Figure 6: *Left panel.* Histogram of the inclination i (deg). *Right panel.* Histogram of the absolute magnitude H . Both the plots are referred to the set of 734 asteroids in the NEODyS Risk List (as of April 2018).

the filtered set contains 6084 virtual impactors, corresponding to 473 asteroids. We then applied a second filter, considering the virtual impactors corresponding to low-inclination asteroids, *i.e.*, $i < 5$ deg, since the discussion below holds in an exact way in the planar case. In the end we analyzed a sample of 5313 virtual impactors with $IP > 2 \cdot 10^{-7}$ and $i < 5$ deg.

For a single asteroid, the accumulation of virtual impactors with time depends on the time elapsed since the first observed close approach. We call this relative time t_{rel} , assuming as origin ($t_{rel} = 0$) the time of the first observed close approach. The exact computation of t_{rel} for each asteroid in the risk list would be complicated, but, by taking into account Figure 6 (right panel), we see that the vast majority of the asteroids in the risk list is composed by very small objects. As a consequence, they can only be discovered during a close approach. For almost all of the asteroids in the risk list the center of the observed arc is thus a good approximation of the origin $t_{rel} = 0$. Thus, for each asteroid in the risk list, we sorted the set of its virtual impactors by time and we computed the relative time of each one of them with respect to the center of the observed arc. Figure 7 is the log-log plot of the cumulative number of virtual impactors up to each value of the relative time (blue and green marks). The log-log plot clearly shows a linear growth, which we try to determine with a linear fit. However, for a more accurate fit we have to cut out the tails of the ostensible line. The tail for low relative times because its contribution is weakened by small number statistics. In the tail for high relative times the growth seems to slow down, but this is due to the fact that the maximum relative time for which the scan for VIs has been performed changes from asteroid to asteroid. Thus we performed the linear fit over a suitable interval $t_1 \leq t_{rel} \leq t_2$. This fit corresponds to a power-law, that is

$$\mathcal{N} = c_2 \cdot t_{rel}^\beta \quad \text{if } t_1 \leq t_{rel} \leq t_2. \quad (9)$$

Choosing $t_1 = 40$ yr and $t_2 = 99$ yr we obtained the estimation $\beta = (3.001 \pm 0.001)$, with a linear correlation coefficient 0.9994. The points marked with green circles in Figure 7 are those selected for the linear fit, and the orange straight line is the resulting best-fit line. The histogram in Figure 8 is the histogram of the number of virtual impactors accumulated up to the relative time. The plot represents the same quantity of Figure 7 with an histogram, but not in a log-log scale. The colors

have the same meaning as for Figure 7: the green part corresponds to the tail of the log-log plot used for the linear fit and the orange line is the best fit power-law. Given the approximations introduced in the model, this fit is remarkably good and identifies the power-law proportional to t_{rel}^3 with very low uncertainty.

The power-law behavior with exponent $\simeq 3$ can be explained using the analytical theory of close encounters as developed in Valsecchi et al. (2003), whose results agree with those of the circular restricted three-body problem (Valsecchi et al., 2018). We consider the target plane coordinates ξ and ζ : the former corresponds to the signed local MOID, whereas the latter is related to the timing of the encounter. We use the wire approximation (Valsecchi et al., 2003; Milani et al., 2005a), that is we assume that the LOV projection on the target plane of a given encounter is a continuous sequence of points, all with the same value of ξ and differing only for the value of ζ . Then, for each asteroid we proceed along the same lines described in the appendix of Spoto et al. (2014).

The condition for a collision at a resonant return to take place is that the ratio of the period of the small body and that of the Earth is k/h , with k and h relatively prime integers. Then, following the first encounter, after h heliocentric revolutions of the small body and k revolutions of the Earth, both the Earth and the small body will be back to the same position (Milani et al., 1999; Valsecchi et al., 2003). This situation means that the post-encounter semimajor axis a' has to have precisely a certain value, say a'_* , with the corresponding mean motion n'_* . For the Kepler's third law, the latter has to be

$$n'_* = \left(\frac{h}{k}\right)^{2/3}. \quad (10)$$

As shown in Valsecchi et al. (2003) and in the appendix of Spoto et al. (2014), the values of a' are constrained between a maximum and a minimum, say a'_{max} and a'_{min} , to which correspond n'_{min} and n'_{max} respectively. Consider now the time interval in which we are interested: since $t_2 \simeq 99$ yr, it is clear that we have to consider all the values of $n'_{min} \leq n' \leq n'_{max}$ that, expressed as in (10), have $k < 99$. Thus the number of collision possibilities, *i.e.*, of virtual impactors, is proportional to the number of encounter opportunities. This number accumulates in the same way as the number of elements of $\mathcal{F}_n^{r,s}$, which is the set of irreducible fractions between two integers r and $s > r$, and whose denominators do not exceed n , called Farey fractions (see Appendix B). Theorem 4 states that the number of elements of $\mathcal{F}_n^{r,s}$ grows like n^2 and that it accumulates as n^3 , which is the result highlighted from the fit of Figure 8.

The above reasoning holds in an exact way, even for a single small body, in the planar circular restricted three-body problem with Jacobi constant \mathcal{J} sufficiently high to ensure the small body will not be expelled on a hyperbolic orbit, *i.e.*, $\mathcal{J} > 2\sqrt{2}$ (Carusi et al., 1982). Of course the hypotheses on which our analytical estimate is based are an approximation of the more complex problem of asteroid close approaches, nevertheless the general trend turns out to be confirmed by our statistical analysis. If we add back to the list of asteroids with VIs (with $IP > 2 \cdot 10^{-7}$) the ones with higher inclination, $i > 5$ deg, the fit for the slope in the log-log plot gives $\beta = 2.829$, indicating that the model we have proposed can represent accurately the statistics of the VIs time distribution only in the low inclination case, as expected.

Note that the slope predicted by the Farey number-theoretical arguments refers to the number of close approaches to the Earth, not to the number of virtual impactors. The fact that the histogram of VIs as a function of t_{rel} follows the same power-law expected for the number of close approaches indicates that, on average, the number of virtual impactors is proportional to the number of close approaches. This is by no means an obvious result. The possibility of an impact during such a

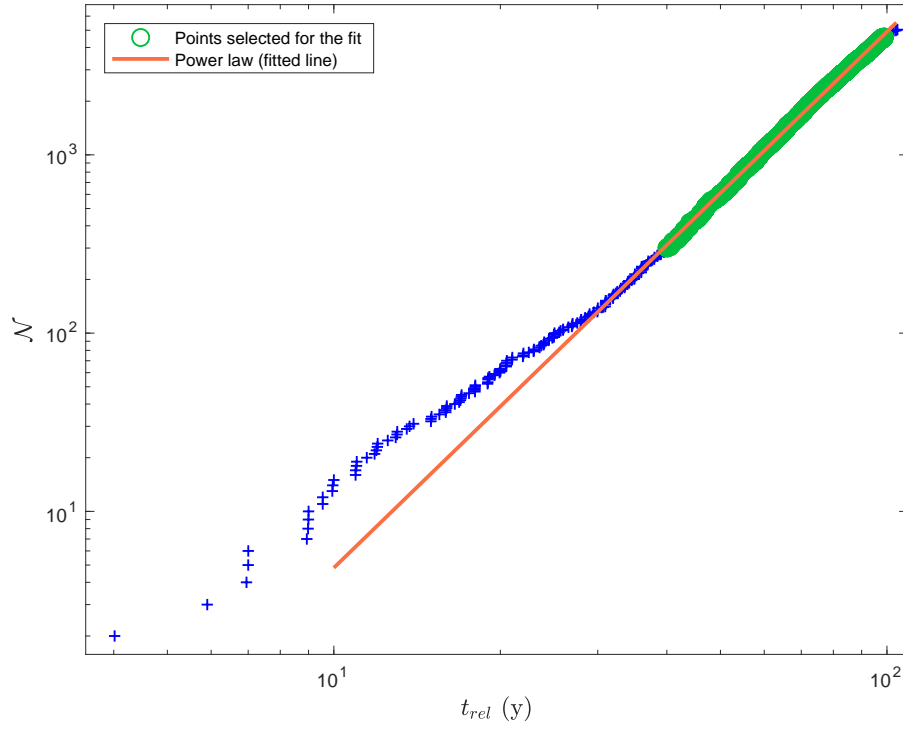


Figure 7: Log-log plot of the cumulative number of virtual impactors \mathcal{N} as a function of the relative time t_{rel} (y). The points selected for the linear fit are marked with green circles. The orange straight line is the best-fit line obtained from the linear fit.

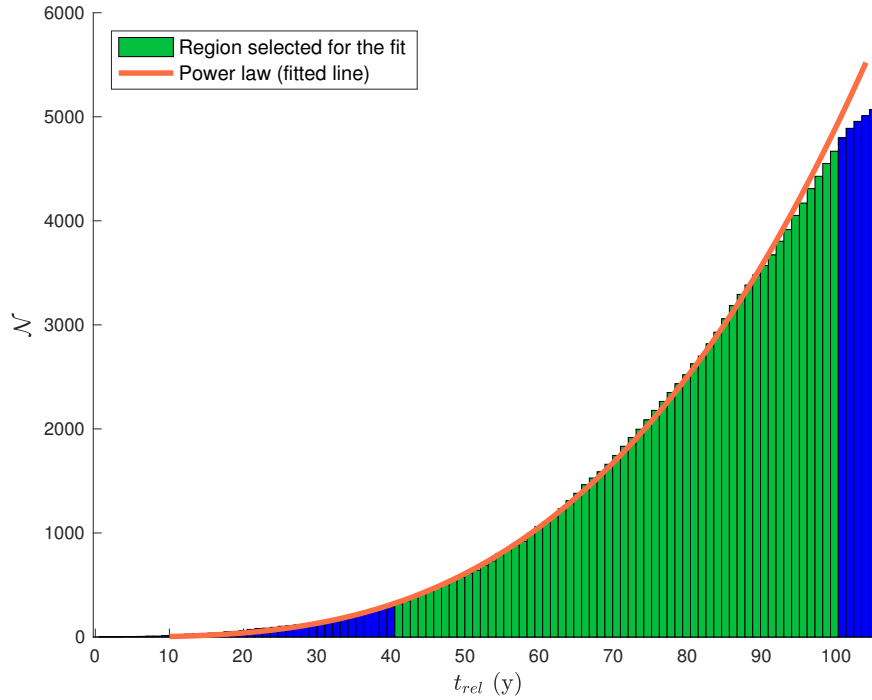


Figure 8: Plot of the cumulative number of virtual impactors \mathcal{N} as a function of the relative time t_{rel} (y).

close approach is controlled by the MOID (Minimum Orbital Intersection Distance) at the time of the encounter: if the MOID is larger than the radius b_{\oplus} of the Earth impact cross section, collisions cannot occur. The MOID changes both as a consequence of short-periodic perturbations and because of secular perturbations slowly changing the MOID through the Lidov-Kozai cycle (Gronchi and Milani, 2001). The empirical finding that the impact probability and the probability of a close approach are proportional, at least as a mean over thousands of cases, would indicate that the MOID can be modeled as a random variable. However, a rigorous mathematical formulation for this is not yet available.

7. Comparison with JPL results

We performed a global comparison between the results of CLOMON-2 and Sentry. An asteroid-by-asteroid comparison is beyond the scope of this paper, thus we present a statistical comparison using histograms like those shown in Section 5. In particular, we take the ensemble of all the virtual impactors computed by CLOMON-2 and Sentry at the same epoch (April 2018). Figure 9 refers to the results of CLOMON-2 and Figure 10 to the ones of Sentry: both plots represent the number of virtual impactors \mathcal{N} as a function of the inverse of the impact probability IP .

Both plots show a very good agreement in the ascending part up to $IP \simeq 2 \cdot IP^* = 2 \cdot 10^{-7}$ (vertical red line). To strengthen this argument we also performed a linear fit of the histogram contour for $IP > IP^*$, as in equation (8). The exponent of the power-law resulted to be $\alpha \simeq 0.664$ for the CLOMON-2 results and $\alpha \simeq 0.679$ for the Sentry results. The number of VIs obtained by Sentry at $IP \simeq 2 \cdot IP^*$ is somewhat lower than our number and it is the cause for the difference in the values of the multiplicative constant c_1 of equation (8) obtained from both fits.

For much lower impact probabilities, the two plots show some differences. The loss of efficiency in the region between the two vertical lines is a common feature, but our histogram is increasing whereas the one related to Sentry begins to slightly decrease. Overall the behavior of the two systems in the detection of VIs with $IP > IP^*$ is very well consistent, which was one of the goals of the improvements in our system. The biggest difference is in the right parts of the histograms: our plot is strictly decreasing, corresponding to the fact that the number of virtual impactors grows but the probability to detect them simultaneously decreases, whereas the histogram related to Sentry shows a peak around $IP \simeq 10^{-9}$. This behavior might be explained by differences in the computation techniques, in particular in the treatment of the off-LOV virtual impactors (Milani et al., 2005a), which usually have very low impact probabilities. We plan to work on these differences in collaboration with the JPL team.

In conclusion, the global comparison confirms a very good agreement between the two systems. The differences we found are mostly explained by technicalities of the methods used in the impact monitoring computations and anyway mostly regard very low probability VIs. Of course this does not exclude differences, in particular in the computed IP for each virtual impactor, which necessarily arise because we are currently using two different error models for the astrometric observations, also taking into account that these error models are incomplete for lack of metadata. The fact that the results for $IP > IP^*$ are very similar in terms of the number of VIs found is a very significant result, precisely because two different error models have been used.

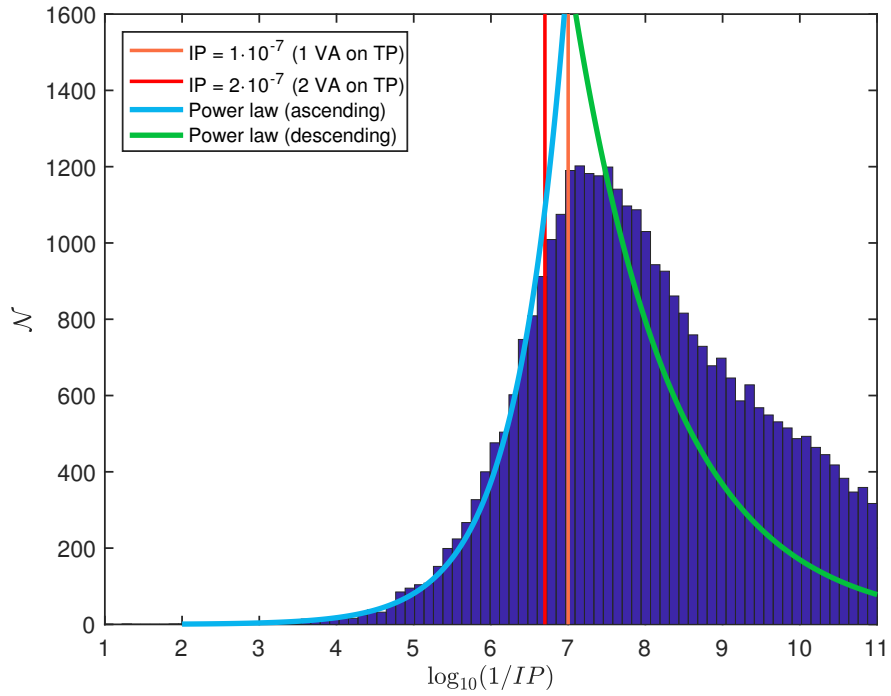


Figure 9: Histogram of the number of virtual impactors in the NEODyS Risk List as a function of the inverse of the impact probability (as of April 2018).

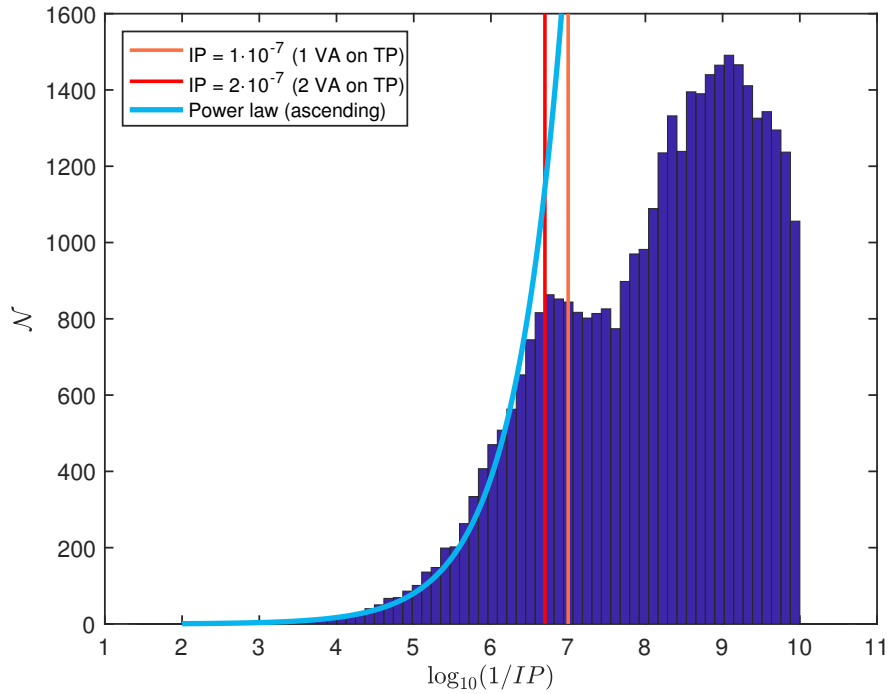


Figure 10: Histogram of the number of virtual impactors in the Sentry Risk List as a function of the inverse of the impact probability (as of April 2018).

8. Conclusion and future work

In this paper we reported on two improvements of our impact monitoring system CLOMON-2 with respect to what was described in (Milani et al., 2005a). The first one was a correct handling of the cases in which a return on the target plane of the Earth includes two instances of the same virtual asteroid. This was done by using a recursive splitting of the showers, thus radically eliminating these duplications. The second was to decrease the impact probability corresponding to the generic completeness, which was previously $\simeq 4 \cdot 10^{-7}$, to $1 \cdot 10^{-7}$. We did not achieve this result by brute force, that is by using four times more virtual asteroids, but by using a sampling of the Line Of Variations optimized by a uniform probability for each segment, at least for the portion closer to the nominal solution.

Both improvements have been implemented in the operational software and fully tested, by recomputing the entire risk list, that is the asteroids known to have VIs. Note that both the improvements we have implemented were removing differences between the algorithm used in the Sentry system of JPL and our CLOMON-2. Thus, having implemented these two improvements, we were for the first time able to perform a full statistical comparison between the global results of CLOMON-2 and those of Sentry, since the two systems should now be giving more similar results.

When we first produced this kind of histograms of the number of VIs found in all the risk list asteroids, as a function of variables such as $1/IP$ and the stretching S , we found empirically that the number of detected virtual impactors with $IP > IP^*$ appeared to grow according to a power-law, proportional to $IP^{-2/3}$. As shown in the figures of this paper, we have tested that this result, numerically quite accurate, was obtained with the risk list as computed with different sampling of the LOV and with different values of IP^* (compare Figure 7 and Figure 8), as computed at different dates (compare Figure 8 and Figure 9), and for risk lists at the same date but computed with different software and different astrometric error models (compare Figure 9 and Figure 10). Thus we are lead to believe that we have experimentally found a fractal property of the set of the initial conditions leading to impacts in the chaotic dynamical system of planet crossing asteroids. We must admit we do not yet have a model explaining this power-law. We suspect it is related to the power-law by which the cumulative number of VIs within a time t_{rel} from the first observed close approach grows proportional to the power-law t_{rel}^3 , for which we have found a number-theoretical argument. However, for the connection between the two power-laws we have not yet found a model, which we suspect to hide in properties of the chaotic orbits of near-Earth asteroids.

Still, the use of the empirical law $IP^{-2/3}$ allows us to explore, for the first time, the effective completeness of the impact monitoring systems: of course this completeness cannot extend beyond the generic completeness limit IP^* . The results are encouraging, in that both CLOMON-2 and Sentry are not just statistically consistent, but also consistent with the empirical power-law, down to an $IP \simeq 2 \cdot 10^{-7}$. This is a significant achievement, because we never had a “ground truth” against which to assess our performance. Since the two impact monitoring systems are currently using two different error models for astrometric observations, by using the standard argument that the difference between the last two models can be considered an estimate of the inaccuracies remaining in the last one, this indicates also robustness of our results with respect to the astrometric error model.

The discussion above clearly indicates the directions we should move in our future work. First, we would like to close the gap between the generic completeness at $IP^* = 10^{-7}$ and the effective completeness (resulting from the comparison with the power-law) at $IP \simeq 2 \cdot 10^{-7}$. In principle we know how to do this by densification of the cases in which a return contains too few points on the

target plane, but we would like to find a solution which is not brute force and this requires some effort, but appears feasible. Second, we need to investigate in depth the issue of the VI histogram power-law, to understand if indeed it is a fractal property and provide at least an approximate model explaining it, possibly starting from the success in explaining the power-law with respect to time. This requires some new idea, thus we are not able to claim that we shall solve this problem, but we shall try. Also other researchers are welcome to try.

Acknowledgments

A. Del Vigna and A. Chessa acknowledges support by the company SpaceDyS. Part of this research was conducted under European Space Agency contract No. 4000113555/15/DMRP “P2-NEO-II Improved NEO Data Processing Capabilities”.

We thank NASA-JPL for making available on their web risk page the data on the virtual impactors found by Sentry, and also for the assistance in downloading the full list. We thank Davide Farnocchia (JPL) for useful discussions, in particular for the comparison between our system and theirs.

We thank the referees (S. Chesley and an anonymous) for suggesting improvements which we think have made easier the understanding of this paper, including the new Figures 2 and 3.

Appendix A. Decomposition of returns with duplications

In this appendix we provide a detailed description of the procedure to decompose a return with duplications into sub-returns, giving a mathematical proof of completion.

A return \mathcal{R} is given by a contiguous LOV segment, that is the indices of the corresponding virtual asteroids are consecutive. Let $\mathcal{I}_{\mathcal{R}}$ be this set of indices. Let $n_{\mathcal{R}}$ the number of distinct close approaches of the return \mathcal{R} . We rigorously define the return to be

$$\mathcal{R} := \{(i_k, t_k) : i_k \in \mathcal{I}_{\mathcal{R}}\}_{k=1, \dots, n_{\mathcal{R}}},$$

considering \mathcal{R} as the set of couples given by the LOV index and the corresponding closest approach time. We also assume that the sequence of times $(t_k)_{k=1, \dots, n_{\mathcal{R}}}$ is non-decreasing, that is $t_{k+1} \geq t_k$ for all k . We now suppose that the return contains a duplication, that is there exist $k_1, k_2 \in \{1, \dots, n_{\mathcal{R}}\}$ such that $k_1 \neq k_2$ and $i_{k_1} = i_{k_2}$, in such a way that the return has to be further decomposed.

For $1 \leq s \leq n_{\mathcal{R}}$ define $I_s := \{i_k : 1 \leq k < s\}$. We now want to recursively define the sequence $(s_n)_{n \geq 1}$ of the beginning points of the sub-showers. Let $s_1 = 1$ and, for $n \geq 0$ define

$$s_{n+1} = \min_{s_n < s \leq n_{\mathcal{R}}} \{s : i_s \in I_s \setminus I_{s_n}\}$$

or $s_{n+1} = n_{\mathcal{R}}$ in case the minimum does not exist because the set is empty. By definition $(s_n)_{n \geq 1}$ is a non-decreasing sequence. Since $s_n \leq N$ for all $n \geq 1$, there exists n_s such that

$$s_1 < s_2 < \dots < s_{n_s} \quad \text{and} \quad s_n = n_{\mathcal{R}} \quad \text{for } n > n_s.$$

The integer n_s is the number of sub-showers in \mathcal{R} . For $1 \leq n \leq n_s$ let $\mathcal{I}_n := I_{s_{n+1}} \setminus I_{s_n}$ be the set of the indices of each sub-shower. Note that the indices in \mathcal{I}_n are pairwise distinct by construction.

Moreover, the collection $\{\mathcal{I}_n\}_{1 \leq n \leq n_s}$ is a partition of $\{1, \dots, n_{\mathcal{R}}\}$. The sub-showers of \mathcal{R} are thus defined to be

$$\mathcal{S}_n := \{(i_k, t_k) : k \in \mathcal{I}_n\}$$

for $1 \leq n \leq n_s$ and

$$\mathcal{R} = \bigsqcup_{n=1}^{n_s} \mathcal{S}_n.$$

There is no guarantee that the indices in a sub-showers are consecutive, thus each sub-shower is further decomposed in sub-returns by taking contiguous LOV segments. Rigorously, for each $1 \leq n \leq n_s$ there exist an integer $r_n \geq 0$ and a collection of r_n subsets $\{\mathcal{R}_{n,m}\}_{m=1, \dots, r_n} \subset \mathcal{S}_n$ such that the indices of $\mathcal{R}_{n,m}$ are a maximal set of consecutive numbers among the indices of \mathcal{S}_n and such that $\mathcal{S}_n = \bigsqcup_{m=1}^{r_n} \mathcal{R}_{n,m}$. In this way we obtain

$$\mathcal{R} = \bigsqcup_{n=1}^{n_s} \bigsqcup_{m=1}^{r_n} \mathcal{R}_{n,m},$$

the decomposition of \mathcal{R} in sub-returns. Given this formal procedure, since the initial number of close approaches contained in starting return is finite, it is proven that the procedure has a finite number of steps, at the end of which there are no duplicate points.

Appendix B. The Farey sequence

The *Farey sequence* \mathcal{F}_n of order n is the ascending sequence of irreducible fractions between 0 and 1 whose denominators do not exceed n . That is, $\frac{h}{k} \in \mathcal{F}_n$ if $0 \leq h \leq k \leq n$ and $(h, k) = 1$ ¹², with the numbers 0 and 1 included in the form $\frac{0}{1}$ and $\frac{1}{1}$. For instance, the elements of \mathcal{F}_5 are the following:

$$\frac{0}{1}, \frac{1}{5}, \frac{1}{4}, \frac{1}{3}, \frac{2}{5}, \frac{1}{2}, \frac{3}{5}, \frac{2}{3}, \frac{3}{4}, \frac{4}{5}, \frac{1}{1}.$$

By definition $\mathcal{F}_{n-1} \subseteq \mathcal{F}_n$ for all $n > 1$, and the smallest Farey sequence is that of order $n = 1$

$$\mathcal{F}_1 = \left\{ \frac{0}{1}, \frac{1}{0} \right\}.$$

The property of the Farey sequence which is important for the result in Section 6 concerns the asymptotic behavior of the number of elements of \mathcal{F}_n . Its proof is can be found in Hardy et al. (2008). First we have to recall the definition of the *Euler totient function* φ . For each integer $n \geq 1$ we define $\varphi(n)$ as the number of positive integers $\leq n$ and relatively prime with n . For instance, $\varphi(1) = 1$, $\varphi(6) = 2$, $\varphi(33) = 20$. There is a simple equation to evaluate φ :

$$\varphi(n) = n \prod_{p|n} \left(1 - \frac{1}{p} \right),$$

where the product is extended to all the prime numbers that divide n .

¹²The symbol (h, k) , with h and k integers, denotes their greatest common divisor.

Theorem 1. *The length of the Farey sequence of order n is*

$$|\mathcal{F}_n| = 1 + \sum_{k=1}^n \varphi(k).$$

The following theorem gives the asymptotic behavior of $|\mathcal{F}_n|$ as $n \rightarrow +\infty$. It can be proved by Theorem 1 and (Hardy et al., 2008, Theorem 330).

Theorem 2. *As $n \rightarrow +\infty$*

$$|\mathcal{F}_n| \sim \frac{3}{\pi^2} n^2.$$

Using the Stoltz-Cesaro theorem we can prove the following statement on the accumulation of $|\mathcal{F}_n|$.

Theorem 3. *As $n \rightarrow +\infty$*

$$\sum_{k=1}^n |\mathcal{F}_k| \sim \frac{1}{\pi^2} n^3.$$

Proof. The sequence $b_n = n^3$ is increasing and $\lim_{n \rightarrow +\infty} b_n = +\infty$. The thesis follows from Theorem 2 and from the Stoltz-Cesaro theorem since

$$\frac{\sum_{k=1}^{n+1} |\mathcal{F}_k| - \sum_{k=1}^n |\mathcal{F}_k|}{(n+1)^3 - n^3} = \frac{|\mathcal{F}_{n+1}|}{3n^2 + 3n + 1} = \frac{|\mathcal{F}_{n+1}|}{(n+1)^2} \frac{(n+1)^2}{3n^2 + 3n + 1} \rightarrow \frac{1}{\pi^2}.$$

□

Analogous results hold in case we consider the irreducible fractions between any two integers r and $s > r$ and with denominator not exceeding n . Let us denote that set of fraction with $\mathcal{F}_n^{r,s}$.

Lemma 1. *Each unit interval $[\ell, \ell + 1]$ contains exactly as many irreducible fractions with denominator not exceeding n as $[0, 1]$. That is, $|\mathcal{F}_n| = |\mathcal{F}_n^{\ell, \ell+1}|$.*

Proof. It suffices to prove that there exists a bijection between \mathcal{F}_n and $\mathcal{F}_n^{\ell, \ell+1}$. If $\frac{h}{k} \in \mathcal{F}_n$, then consider $\frac{h}{k} + \ell$: it belongs to $[\ell, \ell + 1]$ and it is irreducible since $(h, h + k\ell) = 1$ (otherwise $(h, k) > 1$). Thus $\frac{h}{k} + \ell \in \mathcal{F}_n^{\ell, \ell+1}$. Analogously, if $\frac{h}{k} \in \mathcal{F}_n^{\ell, \ell+1}$ then $\frac{h}{k} - \ell$ belongs to $[0, 1]$ and it is irreducible. □

Theorem 4. *For $s > r$ integers, as $n \rightarrow +\infty$*

$$|\mathcal{F}_n^{r,s}| \sim \frac{3(s-r)}{\pi^2} n^2 \quad \text{and} \quad \sum_{k=1}^n |\mathcal{F}_k^{r,s}| \sim \frac{s-r}{\pi^2} n^3.$$

Proof. it is possible to write $[r, s]$ as the union of adjacent unit intervals as $[r, s] = \bigcup_{i=0}^{s-r} [r+i-1, r+i]$. As a consequence and also by applying the above lemma we get

$$|\mathcal{F}_n^{r,s}| = (s-r)|\mathcal{F}_n| - (s-r-1).$$

The thesis follows from Theorem 2. □

References

- Carusi, A., Kresák, L., Valsecchi, G. B., 1982. Orbital patterns of interplanetary objects at close encounters with Jupiter. *Bulletin of the Astronomical Institutes of Czechoslovakia* 33, 141–150.
- Chesley, S. R., Chodas, P. W., Milani, A., Valsecchi, G. B., Yeomans, D. K., 2002. Quantifying the Risk Posed by Potential Earth Impacts. *Icarus* 159, 423–432.
- Chesley, S. R., Farnocchia, D., Pravec, P., Vokrouhlický, D., 2016. Direct Detections of the Yarkovsky Effect: Status and Outlook. In: Chesley, S. R., Morbidelli, A., Jedicke, R., Farnocchia, D. (Eds.), *Asteroids: New Observations, New Models*. Vol. 318 of IAU Symposium. pp. 250–258.
- Chodas, P. W., Yeomans, D. K., 1996. The orbital motion and impact circumstances of Comet Shoemaker-Levy 9. In: Noll, K. S., Weaver, H. A., Feldman, P. D. (Eds.), *IAU Colloq. 156: The Collision of Comet Shoemaker-Levy 9 and Jupiter*. pp. 1–30.
- Del Vigna, A., Faggioli, L., Spoto, F., Milani, A., Farnocchia, D., Carry, B., 2018. Detecting the Yarkovsky effect among near-Earth asteroids from astrometric data. *Astronomy & Astrophysics*. *Submitted*.
- Farnocchia, D., Chesley, S. R., Micheli, M., 2015. Systematic ranging and late warning asteroid impacts. *Icarus* 258, 18–27.
- Farnocchia, D., Chesley, S. R., Vokrouhlický, D., Milani, A., Spoto, D., Bottke, W. F., 2013. Near earth asteroids with measurable yarkovsky effect. *Icarus* 224, 1–13.
- Gronchi, G. F., Milani, A., 2001. Proper Elements for Earth-Crossing Asteroids. *Icarus* 152, 58–69.
- Hardy, G., Wright, E., Heath-Brown, R., Silverman, J., 2008. *An Introduction to the Theory of Numbers*. Oxford mathematics. OUP Oxford.
- Milani, A., 1999. The Asteroid Identification Problem. I. Recovery of Lost Asteroids. *Icarus* 137, 269–292.
- Milani, A., Chesley, S., Boattini, A., Valsecchi, G. B., 2000. Virtual impactors: search and destroy. *Icarus* 145(1), 12–24.
- Milani, A., Chesley, S., Sansaturio, M. E., Tommei, G., Valsecchi, G. B., 2005a. Nonlinear impact monitoring: line of variation searches for impactors. *Icarus* 173, 362–384.
- Milani, A., Chesley, S. R., Valsecchi, G. B., 1999. Close approaches of asteroid 1999 an10: resonant and non-resonant returns. *Astronomy & Astrophysics* 346, L65–L68.
- Milani, A., Gronchi, G. F., 2010. *Theory of Orbit Determination*. Cambridge University Press.
- Milani, A., Sansaturio, M., Tommei, G., Arratia, O., Chesley, S. R., 2005b. Multiple solutions for asteroid orbits: Computational procedure and applications. *Astronomy & Astrophysics* 431, 729–746.
- Spoto, F., Del Vigna, A., Milani, A., Tommei, G., Tanga, P., Mignard, F., Carry, B., Thuillot, W., David, P., 2018. Short arc orbit determination and imminent impactors in the Gaia era. *Astronomy & Astrophysics*. *Accepted for publication*.

- Spoto, F., Milani, A., Farnocchia, D., Chesley, S. R., Micheli, M., Valsecchi, G. B., Perna, D., Hainaut, O., 2014. Nongravitational perturbations and virtual impactors: the case of asteroid (410777) 2009 FD. *Astronomy & Astrophysics* 572.
- Tommei, G., 2005. Nonlinear impact monitoring: 2-dimensional sampling. In: Milani, A., Knežević, Z. (Eds.), *IAU Colloquium 197: Dynamics of Populations of Planetary Systems*. Cambridge University Press, pp. 259–264.
- Tommei, G., 2006. Impact monitoring of neos: theoretical and computational results. Ph.D. thesis, University of Pisa.
- Valsecchi, G. B., Alessi, E. M., Rossi, A., 2018. Cartography of the b-plane of a close encounter I: semimajor axes of post-encounter orbits. *Celestial Mechanics and Dynamical Astronomy* 130, 8.
- Valsecchi, G. B., Milani, A., Gronchi, G. F., Chesley, S. R., 2003. Resonant returns to close approaches: Analytical theory. *Astronomy & Astrophysics* 408, 1179–1196.